

PCCP

Accepted Manuscript



This is an *Accepted Manuscript*, which has been through the Royal Society of Chemistry peer review process and has been accepted for publication.

Accepted Manuscripts are published online shortly after acceptance, before technical editing, formatting and proof reading. Using this free service, authors can make their results available to the community, in citable form, before we publish the edited article. We will replace this *Accepted Manuscript* with the edited and formatted *Advance Article* as soon as it is available.

You can find more information about *Accepted Manuscripts* in the [Information for Authors](#).

Please note that technical editing may introduce minor changes to the text and/or graphics, which may alter content. The journal's standard [Terms & Conditions](#) and the [Ethical guidelines](#) still apply. In no event shall the Royal Society of Chemistry be held responsible for any errors or omissions in this *Accepted Manuscript* or any consequences arising from the use of any information it contains.

Cite this: DOI: 10.1039/xxxxxxxxxx

Flexible magnetic filaments under the influence of external magnetic fields in the limit of infinite dilution.

Joan J. Cerdà,^{*a‡} Pedro A. Sánchez,^b Daniel Lüsebrink,^{ac} Sofia Kantorovich,^{bd} and Tomàs Sintès^a

Received Date
Accepted Date

DOI: 10.1039/xxxxxxxxxx

www.rsc.org/journalname

In the present work we use Langevin dynamics computer simulations to understand how the presence of a constant external magnetic field modifies the conformational phase diagram of magnetic filaments in the limit of infinite dilution. We have considered the filament immersed in either a good (non-sticky filaments) or a poor (Stockmayer polymers) solvent. It has been found that in the presence of an applied field, filaments turn out to be much more susceptible to parameters such as temperature and solvent conditions. Filaments owe this increased susceptibility to the fact that the external magnetic field tends to level the free energy landscape as compared to the zero-field case. The field induces an equalization in the free energy of competing conformational states that were separated by large energy differences in the zero-field limit. In this new scenario multistability arises, and manifests itself in the existence of broad regions in the phase diagram where two or more equilibrium configurations coexist. The existence of multistability greatly enhances the possibility of tuning the properties of the filament.

1 Introduction

Magnetic filaments are a scaled up version at a supra-molecular level of magnetic polymers. These filaments are created using magnetic particles linked one after another in a linear sequence to form a permanent chain. Several methods have been reported in the literature in order to link sequentially the magnetic monomers^{1–16}.

In difference to the true chemical polymers, that generally can only exhibit their magnetic properties at temperatures below $T < 100\text{K}$ ^{17,18}, magnetic filaments can retain their magnetisation above room temperature if the material and size of the nano-colloids is chosen adequately to be ferromagnetic. The current growing interest in the area of magnetic filaments is driven by their potential use in technological applications like microfluidics or as substitutes for current ferrofluids with improved properties, elements for magnetic information storage, as well as pressure and chemical nanosensors to mention just a few¹¹. In turn, 'inverse magnetic filaments' have already proven to be useful in the assembly of non-permanent photonic crystals¹⁹. In most of

these applications an external magnetic field is applied to control magneto-responsive materials. Therefore, it is extremely important to understand different types of equilibrium configurations that filaments may assume as a function of the field and the interactions among the magnetic nanoparticles.

The behaviour of paramagnetic and super-paramagnetic non-sticky chains under an external field were already thoroughly studied several years ago as promising candidates for micro-propellers (micro-swimmers)^{10,20–29}. Paramagnetic and super-paramagnetic chains opened up a new possibility to design magneto-responsive actuators^{4,30} at the nanoscale, similar to those of micro-metric cilia^{31,32} or responsive brushes³³. Most of these studies treated the filaments as elastic rods in which the direction and strength of the magnetic dipoles were induced by the oscillating external field. Another model was proposed to study polyelectrolyte chains with electric dipoles³⁴, but their properties were found to be drastically different from those of magnetic filaments³⁵. To our best knowledge, filaments made of ferromagnetic particles, being potentially easy to control with externally applied magnetic fields, have received far less attention.

In the case of absence of external magnetic field, these filaments have been studied in several recent works. Very recently Stankovic et al. have addressed the problem of magnetic filaments in a confining cylindrical surface³⁶. In the case of chains in the bulk or near a wall also some studies are available^{37–44}. The behaviour of a filament under these conditions is determined by three main parameters: the ratio between the magnetic en-

^a Instituto de Física Interdisciplinar y Sistemas Complejos, IFISC (CSIC-UIB). Universitat de les Illes Balears. E-07122 Palma de Mallorca, Spain.

^b Faculty of Physics. University of Vienna. Boltzmannngasse, 5, 1090 Vienna, Austria.

^c UCB Department of Physics and Astronomy, University of British Columbia, 6224 Agricultural Road Vancouver, B.C. V6T 1Z1, Canada.

^d Institute of Mathematics and Applied Informatics. Ural Federal University. Lenin av, 51, 620000, Ekaterinburg, Russia.

‡ E-mail: joan@ifisc.uib-csic.es

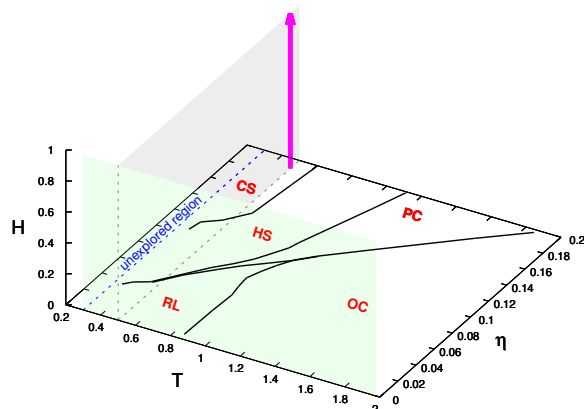


Fig. 1 Schematic representation of the phase diagram previously derived at $H = 0$ for a filament length $N = 100$ and a magnetic dipole strength $\mu^2 = 5$ in the absence of an external magnetic field⁴⁴. The parameter η , defined in eq. 7, measures the relative strength of the non-magnetic and the magnetic interactions for two monomers in close contact. In the plane $H = 0$, the label *OC* stands for the open chain state region, *RL* depicts the region of closed ring-like states, *PC* corresponds to partially collapsed states, *HS* stands for compact closed helicoidal structures, and *CS* marks the region where compact globule structures were found to exist. An explanation of the vertical planes is provided in the main text.

ergy and the thermal fluctuations, the type of the cross-linking bond, and the short range isotropic interactions among the particles in the chain. The first parameter was actively studied in various analytical and simulation works^{37–41,43}. The influence of the type of the crosslinking bond on the magnetic correlations within the chain was also analysed^{42,43}. Finally, the existence of a short range attraction among the magnetic particles was thoroughly investigated by Cerdà et al.⁴⁴, where the authors obtained the structural phase diagram included in Figure 1 as a horizontal zero external field plane ($H = 0$). In this phase diagram, filament conformations are presented as a function of two dimensionless control parameters: the ratio of the isotropic attraction energy to the magnetic one, η , and T , which denotes the dimensionless temperature in the system. More details on how the reduced units are defined in the present study can be found in the next section. Several unusual conformations were unveiled while calculating the $H = 0$ part of the diagram in Figure 1, like closed helicoidal and partially collapsed states, in addition to the already known open chains and ring-like structures. Some of these conformational phases were observed to coexist in two “triple-points”⁴⁴.

In this work, we add an extra control parameter to the aforementioned phase diagram by studying in detail the influence of the external magnetic field on the equilibrium configurations of a magnetic filament at different points of the $\eta - T$ parameter’s space. The two coloured planes and the purple line in Figure 1 indicate the different regions for $H > 0$ that are discussed in this work in order to exemplify our findings: the plane $\eta = 0$ corresponds to the case of non-sticky filaments, and the plane $T = 0.5$ corresponds to a selected sample of Stockmayer filaments

at low temperatures and moderate fields. The purple arrow indicates that for $(T = 0.5, \eta = 0.2)$ systems have been sampled up to $H = 5$ in order to understand how compact globules behave when a strong magnetic field is applied.

The manuscript is organised in the following way. In the next section, the numerical model and the details of the simulations are described. The main findings are provided in section 3 and are split into two subsections: non-sticky and sticky filaments, respectively. Finally, the summary of our main results is provided in section 4.

2 Numerical Model

We study filaments composed by N ferromagnetic particles, represented as beads permanently linked by an elastic bonding potential. All particles have the same diameter σ_e . Henceforth, the subindex e for any dimensional quantity denotes an experimental value, whereas the absence of such a subindex means that the quantity is expressed in reduced units. The latter are very convenient to ease the transferability of the simulation results. Thus, all lengths in this study are expressed in units of the monomer diameter, i.e. $l = l_e/\sigma_e$, so that the reduced diameter of the filament bead is $\sigma = 1$. In experiments, the size of the nanoparticle usually does not exceed 50 nm. All short range isotropic interactions in the present model are of Lennard-Jones (LJ) type:

$$U_{\text{LJ}}(r_e; \epsilon_e, \sigma_e) = 4\epsilon_e[(\sigma_e/r_e)^{12} - (\sigma_e/r_e)^6], \quad (1)$$

where the prefactor ϵ_e stands for the characteristic energy scale of the isotropic short-range interactions in the system. We take this prefactor as the unit of energy, so that any other energy U_e will be expressed in reduced units as $U = U_e/\epsilon_e$. In particular, to mimic the impenetrability of sterically stabilised magnetic nanoparticles, we chose the simplest form of the Weeks-Chandler-Andersen potential,⁴⁵ which is a LJ potential truncated and shifted in order to make it purely repulsive:

$$U_{\text{WCA}}(r) = \begin{cases} 4[r^{-12} - r^{-6} + 1/4], & \text{for } r < 2^{1/6} \\ 0, & \text{for } r \geq 2^{1/6} \end{cases}, \quad (2)$$

where r is the reduced distance between the centres of the particles i and j , i.e. $r = |\mathbf{r}_i - \mathbf{r}_j|$.

A point dipole $\boldsymbol{\mu}_e$ is assigned to each bead, and located in its centre. The dipole is fixed within the particle body, so that its rotation is impossible without the rotation of the whole bead. The modulus of the magnetic moments in the reduced units is calculated from the following relation: $\mu^2 = \mu_e^2/(\sigma_e^3 \epsilon_e)$, where $|\mu^2| = \mu$. There are two types of magnetic interactions in the system. The first one is the magnetic dipole-dipole interaction:

$$U_{\text{dip}}(\mathbf{r}_{ij}; \boldsymbol{\mu}_i, \boldsymbol{\mu}_j) = \frac{\boldsymbol{\mu}_i \cdot \boldsymbol{\mu}_j}{r^3} - \frac{3[\boldsymbol{\mu}_i \cdot \mathbf{r}_{ij}][\boldsymbol{\mu}_j \cdot \mathbf{r}_{ij}]}{r^5}, \quad (3)$$

where $\mathbf{r}_{ij} = \mathbf{r}_i - \mathbf{r}_j$ is the displacement vector between particles i and j . Reasonable values of $\mu = |\boldsymbol{\mu}|$ depend in general on the composition and size of the nanoparticles, but in usual ferrofluids typically do not exceed values of $\mu_e^2/(kT_e \sigma_e^3) \sim 10$. Here, T_e is the actual temperature of the sample and k is the Boltzmann constant. In our model, we use the reduced temperature $T = kT_e/\epsilon_e$. The

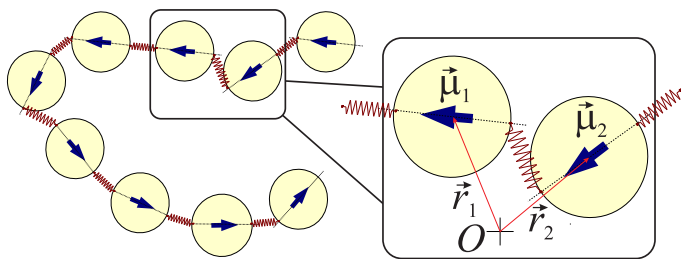


Fig. 2 Schematic representation of the bond-dipole coupling model. Dipole moments are depicted as arrows. The crosslinking do not only constrain the interparticle distance but also the relative orientation of the dipoles. The anchoring points for each colloid are given by $\pm(\sigma/2)\hat{\mathbf{u}}$ where $\hat{\mathbf{u}} = \boldsymbol{\mu}/\mu$ and the centre of the colloids is taken as the origin. The interacting potential is given in eq. 5.

other magnetic interaction considered in this study stems from the presence of an external magnetic field \mathbf{H}_e . Its orientation will be kept fixed along the z-direction, so that in reduced units $\mathbf{H} = (0, 0, H)$, where $H = H_e \sqrt{\sigma_e^3 / (\epsilon_e)}$. Therefore, the Zeeman energy can be written as:

$$U_H(\mathbf{H}, \{\boldsymbol{\mu}_i\}) = - \sum_{i=0}^N \mathbf{H} \cdot \boldsymbol{\mu}_i = -H \sum_{i=0}^N \mu_{zi}. \quad (4)$$

In order to connect the colloids to form a permanent chain, a linking model in which springs between consecutive particles are anchored at fixed points on their surface has been implemented.^{42,44} In this model, as shown in Figure 2, the rotation of the dipole moments away from the filament backbone is penalised by the mechanical stretching of the springs. Therefore, head-to-tail conformations of the dipoles in the chain are favoured not only by the dipole-dipole interaction, but also by the permanent links. This approach closely corresponds to the experimental way of crosslinking ferromagnetic colloids by means of polymer molecules that are end-grafted to the surface of neighbour particles in the chain^{15,46,47}. The spring potential corresponding to this type of elastic bond is:

$$U_B(\mathbf{r}_i, \mathbf{r}_j, \hat{\mathbf{u}}_i, \hat{\mathbf{u}}_j) = \frac{1}{2} K_S \left(\mathbf{r}_i - \mathbf{r}_j - (\hat{\mathbf{u}}_i + \hat{\mathbf{u}}_j) \frac{\sigma}{2} \right)^2, \quad (5)$$

where \mathbf{r}_i and \mathbf{r}_j are the position vectors of the centres of the beads. $\hat{\mathbf{u}}_i$ and $\hat{\mathbf{u}}_j$ are unitary vectors placed along the direction that joins the two anchoring surface points of each bead (see Figure 2). Thus, the anchoring points are collinear and located at $\mathbf{l}'_i = \hat{\mathbf{u}}_i \sigma / 2$ and $\mathbf{l}_i = -\hat{\mathbf{u}}_i \sigma / 2$ with respect to the centre of the bead. All links in the chain are assumed to be formed according to the following scheme: the point on the surface of the $i-1$ particle with position $\mathbf{r}_{i-1} + \mathbf{l}'_{i-1}$ is linked to the point on the surface of the particle i with position $\mathbf{r}_i + \mathbf{l}_i$. In order to penalise those conformations with consecutive dipoles in anti-parallel configuration, each vector director $\hat{\mathbf{u}}_i$ is associated with the magnetic moment of the particle, $\boldsymbol{\mu}_i$, i.e. $\hat{\mathbf{u}}_i = \boldsymbol{\mu}_i / |\boldsymbol{\mu}_i|$. The constant of the potential is set to $K_S = 30$, which results in the average bond length being within a range $r_{bond} \in [0.98, 1.1]$.

Along with steric repulsion, we allow the possibility of a central attraction between filament beads to mimic the effects of

poor solvents (Stockmayer polymers, often referred as “sticky chains”). This interaction is also modelled as a truncated and shifted Lennard-Jones potential (1) with a cutoff $r_{cut} = 2.5$:

$$U_S(r; \epsilon) = \begin{cases} U_{LJ}(r; \epsilon, 1) - U_{LJ}(2.5; \epsilon, 1), & \text{for } r < 2.5 \\ 0, & \text{for } r \geq 2.5 \end{cases} \quad (6)$$

This potential exhibits a typical shallow well of depth $\epsilon = \epsilon_S / \epsilon_e$, where ϵ_S is the experimental value of the central interparticle attraction. Even though this potential has a repulsive part at small distances, the strength of this repulsion is much smaller than that provided at the same distance by the $U_{WCA}(r)$ from eq. 2. For fair comparison of the sticky and non sticky filaments, however, it is essential to provide a similar repulsive interaction at short range, that is why we choose to use either U_{WCA} for non-sticky case, or the sum $U_S + U_{WCA}$ otherwise. The parameter ϵ enters the definition of the dimensionless parameter η used to represent the phase diagram in Figure 1:

$$\eta \equiv \frac{\epsilon \sigma^3}{\mu^2}. \quad (7)$$

This expression characterises the relative strength of the attractive LJ interaction with respect to the strength of the largest magnetic interaction between two particles: close contact, $r_{ij} = \sigma$, and dipoles oriented in a nose-tail conformation. Two dipoles i and j are said to be in a nose-tail conformation when $\boldsymbol{\mu}_i \cdot \boldsymbol{\mu}_j = \mu^2$, and $\boldsymbol{\mu}_i \cdot \mathbf{r}_{ij} = \boldsymbol{\mu}_j \cdot \mathbf{r}_{ij} = \pm \mu r_{ij}$. The nose-tail alignment is the conformation that minimises the magnetic energy in eq.(3).

The numerical simulations are performed using Langevin dynamics. In this approach, the colloidal particles are moved according to the translational and rotational Langevin equations of motion that, for a given particle i , are⁴⁸:

$$M_i \frac{d\mathbf{v}_i}{dt} = \mathbf{F}_i - \Gamma_T \mathbf{v}_i + \boldsymbol{\xi}_i^T \quad (8)$$

$$\mathbf{I}_i \cdot \frac{d\boldsymbol{\omega}_i}{dt} = \boldsymbol{\tau}_i - \Gamma_R \boldsymbol{\omega}_i + \boldsymbol{\xi}_i^R \quad (9)$$

where \mathbf{F}_i , and $\boldsymbol{\tau}_i$ are respectively the total force and torque acting on the particle i . The magnetic component of the torque, $\boldsymbol{\tau}_i^{(mag)}$, can be computed as

$$\boldsymbol{\tau}_i^{(mag)} = -\boldsymbol{\mu}_i \times \nabla_{\boldsymbol{\mu}_i} (U_{dip} + U_H). \quad (10)$$

M_i and \mathbf{I}_i are the mass and the inertia tensor of the colloid, and Γ_T and Γ_R are the translational and rotational friction constants. $\boldsymbol{\xi}_i^T$ and $\boldsymbol{\xi}_i^R$ are Gaussian random forces and torques, each of zero mean value and satisfying the usual fluctuation-dissipation relations

$$\langle \xi_{i\alpha}^T(t) \xi_{j\beta}^T(t') \rangle = 2kT\Gamma_T \delta_{ij} \delta_{\alpha\beta} \delta(t-t'), \quad (11)$$

$$\langle \xi_{i\alpha}^R(t) \xi_{j\beta}^R(t') \rangle = 2kT\Gamma_R \delta_{ij} \delta_{\alpha\beta} \delta(t-t'), \quad (12)$$

where α and β denote x, y, z for translation and rotation in Cartesian coordinates. Equations of motion 8 and 9 are a reasonable approach as far as the size of particles is such that sedimentation forces are negligible. In the simulations, $t = t_e \sqrt{\epsilon_e / (m_e \sigma_e^2)}$, where

m_e is the real mass of the colloids; $F = F_e \sigma_e / \epsilon_e$, and $\tau = \tau_e / \epsilon_e$. For equilibrium simulations, the values of the mass, the inertia tensor, as well as friction constants Γ_T , and Γ_R are irrelevant because the same equilibrium state is reached independently of their value. Only the dynamics to attain such equilibrium state may show differences. For simplicity, the particle mass is chosen to be $m = 1$ and the inertia tensor is chosen to be the identity matrix in order to ensure isotropic rotations $\mathbf{I} = \mathbf{1}$. It has been also chosen $\Gamma_T = 1$ and $\Gamma_R = 3/4$ because these values have been observed to produce a conveniently fast relaxation to equilibrium^{49,50}. The reduced time step is set to $\delta t = 5 \cdot 10^{-4}$ in order to ensure a correct integration of the equations of motion.

Simulations are performed as follows: the magnetic chain is randomly placed in an open three-dimensional non-bounded space and it is pre-equilibrated at $T = 1$ for $2 \cdot 10^5$ integrations with the magnetic interaction turned off while the time step is slowly increased from $10^{-3} \delta t$ to $0.05 \delta t$. Right after, magnetic interactions are turned on, and the second pre-equilibration stage, consisting of $5 \cdot 10^5$ integrations, is performed while gradually raising the time step from $10^{-4} \delta t$ to δt . Magnetic interactions are calculated by direct summation over all pairs of particles. In spite of being algorithmically $\mathcal{O}(N^2)$, for small numbers of colloids this is the fastest and the most accurate way to compute magnetostatic energy in open boundary conditions. Subsequently, if the final temperature of the system is $T < 1$, an annealing process using the final time step δt is performed: the temperature is reduced from $T = 1$ down to its final value by performing a set of five annealing cycles of $5 \cdot 10^5$ steps each. Once the final temperature has been reached, the chain is equilibrated for a period of $2 \cdot 10^6 e^{1/T} \delta t$ in order to ensure that the chain has reached the thermodynamic equilibrium regime. After the equilibration period, the system is sampled at intervals of $10^4 e^{1/T} \delta t$ for another period of $6 \cdot 10^6 e^{1/T} \delta t$ so that correlations between sampled configurations are negligible. To make sure that the results do not depend on the initial conditions and to improve statistics, we additionally average each set of sampled parameters (T, ϵ, μ, H) over 15 independent runs. The simulations have been performed using the package ESPResSo⁵¹.

3 Results and discussion

As a starting point we will consider the conformational phase diagram for $H = 0$, $N = 100$ and $\mu^2 = 5$ represented in Figure 1. Several well defined conformational phases exist in different regions of the $\eta - T$ space: open and closed (ring-like) chains, partially collapsed and helicoidal closed chains, as well as compact disordered globules. The regions corresponding to values of $\eta > 0.2$ or $T < 0.25$ (see, Figure 1) are characterised by structures whose effective sampling demands for special simulation methods^{48,52-55}. In those cases a simple Langevin dynamics approach cannot provide reliable results with reasonable computational resources. Therefore, in the present study, we will exclusively analyse the region of $\eta \leq 0.2$ and $T > 0.2$. Since the lowest explored T is rather high, we do not expect to observe directly any actual 2D⁵⁶ or 3D⁵⁷ ground state structures formed by dipolar hard spheres.

A first insight into the structural changes experienced by mag-

netic filaments in the bulk can be obtained by measuring the radius of gyration, R_g , and the end-to-end distance, R_{ee} , of the magnetic chains. R_{ee} is defined as the distance between the centres of the two end-beads, and its average value is calculated as $\bar{R}_{ee} = \langle |\mathbf{r}_1 - \mathbf{r}_N| \rangle$ where $\langle \dots \rangle$ denotes an average over all the sampled conformations of the chain. The averaged radius of gyration is computed as $\bar{R}_g = \sqrt{\langle R_g^2 \rangle} = \sqrt{\lambda_1^2 + \lambda_2^2 + \lambda_3^2}$, where $\lambda_1^2 > \lambda_2^2 > \lambda_3^2$ are the three eigenvalues or principal moments of the gyration tensor, a 3×3 matrix whose elements are defined as

$$R_{\alpha,\beta} = \frac{1}{2N^2} \left\langle \sum_{i,j=1}^N (r_{i,\alpha} - r_{j,\alpha})(r_{i,\beta} - r_{j,\beta}) \right\rangle, \quad (13)$$

where α and β denotes the Cartesian components x , y , and z .

Simulations show that the behaviour of a filament depends strongly whether the monomers are sticky (Stockmayer, $\eta > 0$) or non-sticky (pure soft-core, $\eta = 0$). Therefore it is advisable to study both cases separately: section 3.1 will be devoted to the study of non-sticky filaments, while section 3.2 will deal with the case of Stockmayer (sticky) chains.

3.1 Non-sticky magnetic filaments ($\eta = 0$)

The behaviour of \bar{R}_{ee} and \bar{R}_g for non-sticky chains is shown in Figure 3. At $H = 0$ our results are in agreement with previous findings^{41,44}. In the high temperature limit ($T > 1.5$) chains behave as self-avoiding random coils. It is possible to identify different regimes as the temperature is lowered from $T = 1.5$ to $T = 0.2$. An initial increase of the averaged values of \bar{R}_{ee} and \bar{R}_g is observed due to an improved nose-tail alignment of the dipoles associated to a diminution of dipole fluctuations. A further lowering of the temperature leads to a contraction of the chain. This contraction is due to the transformation of the open structures into closed ring-like conformations. The subsequent expansion observed in the \bar{R}_g at lower temperatures is related to the tendency of those closed structures to approach the shape of an ideal two-dimensional ring in the limit $T \rightarrow 0$.

For $H > 0$, Figure 3 points out the existence of a field threshold (solid red line) above which the results are clearly different from the zero-field case, specially at low temperatures. The role of the external field can be better understood through the evaluation of the probabilities $P_{R_g}(x)$ and $P_{R_{ee}}(x)$ of finding the filament in a conformation having a value x for R_g and R_{ee} , respectively. Figure 4(a) depicts the probability density function (pdf) of the radius of gyration $f_{R_g}(x) = P(x < R_g < x + dx)$, and the Figure 4(b) shows the cumulative distribution function for the end-to-end observable $F_{R_{ee}}(x) = P(R_{ee} < x)$.

At zero-field, $H = 0$, the pdfs $f_{R_g}(x)$, in all the range of temperatures studied, are single peaked functions. The results for $T \leq 0.7$ correspond to closed-structures, whereas open chain configurations are found for $T > 0.7$. This result is evidenced in the cumulative distribution function $F_{R_{ee}}(x)$ in which $F_{R_{ee}}(x \gtrsim 1) \approx 1$ for $T \leq 0.7$ and $F_{R_{ee}}(x \approx 1) \rightarrow 0$ for $T > 0.7$. For increasing values of the field, $H \geq 0.02$, a bimodal probability distribution is found in $f_{R_g}(x)$. A second peak emerges at larger values of R_g , for the $T \leq 0.7$ curves, corresponding to open-straightened chains.

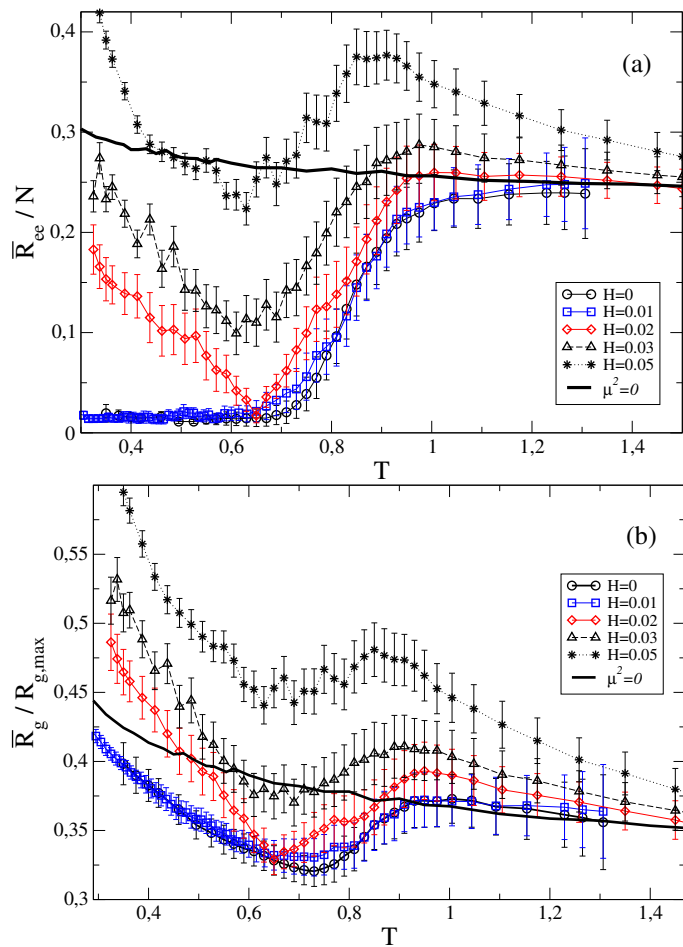


Fig. 3 (a) Normalised average end-to-end distance, \bar{R}_{ce}/N as a function of the temperature, T . (b) Normalised average radius of gyration, $\bar{R}_g/R_{g,max}$ vs. T . Results are for non-sticky ($\eta = 0$) filaments with a length $N = 100$ that have a maximum gyration radius (ideal rod) $R_{g,max} = 28.866\sigma$. The dipole interaction strength is set to $\mu^2 = 5$. The case of non-magnetic chains (thick solid black line) is included for the sake of comparison. Error bars for $\mu^2 = 5$ series are plotted with a confidence interval of 95%. In the case of non-magnetic chains, $\mu^2 = 0$, error bars are roughly of the order of the line thickness and have been skipped.

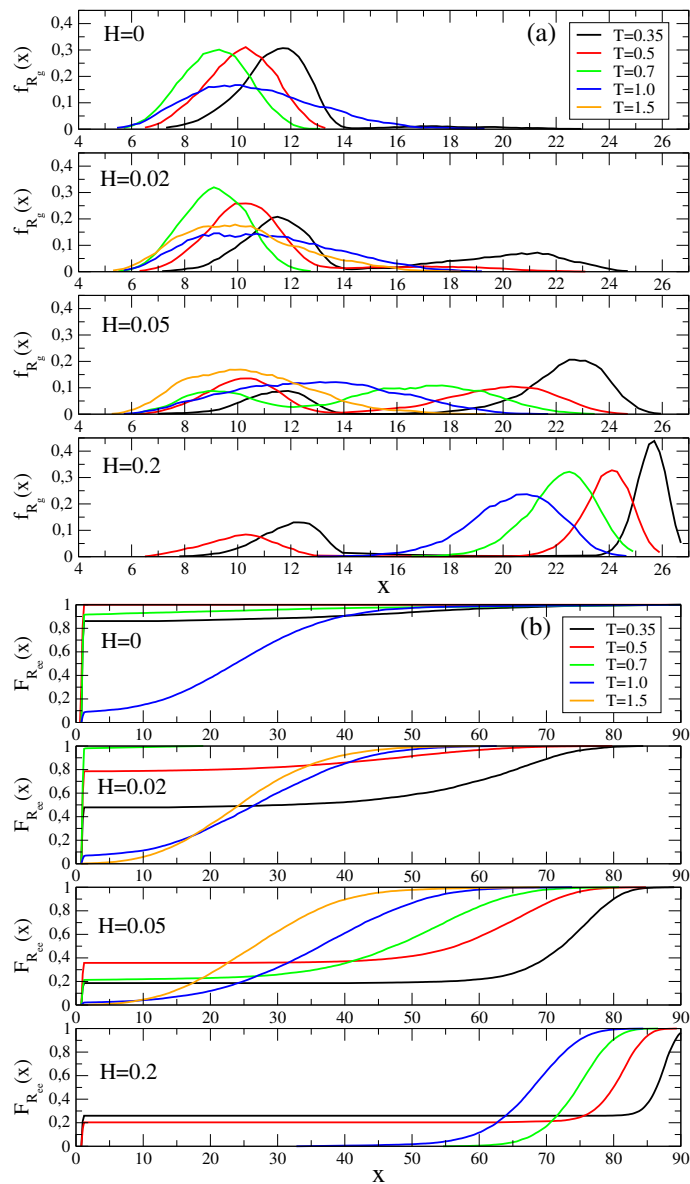


Fig. 4 (a) Probability density function of the radius of gyration $f_{R_g}(x)$ for a chain of length $N = 100$ and $\mu^2 = 5$, as a function of the temperature T and for different values of the external magnetic field H . (b) Cumulative distribution function for the end-to-end distance $F_{R_{ce}}(x)$ for the same system. Note that for $H = 0$ and $H = 0.2$, the data for $T = 1.5$ is not included in the plots.

Therefore, it should be concluded that the presence of an external field promotes the emergence of a bistable region in which it is possible to observe how a magnetic filament fluctuates between two different conformations: open-stretched and ring-like structures. In this regime $F_{Re}(x \approx 1) < 1$ and its value diminishes for increasing values of H . At values of H large enough, the bistability is lost in favour of the open configurations in which the chain stretches along the field. This is the case for $T = 0.7$ at $H = 0.2$ (green line in Figure 4).

The rationale behind the bistability promoted by the external field can be easily understood. At zero field and low temperatures the free energy difference between open and closed chain conformations is very large, and the equilibrium between both kinds of structures is completely biased in favour of the formation of ring-like conformations. Instead, when the field is present, the Zeeman contribution to the free energy of open chains drastically reduces the free energy difference to the point where a reversible equilibria between both types of states can be observed for moderate values of the field. As the strength of the field is increased, the equilibrium will progressively bias in favour of the formation of open-stretched structures.

The complete $T - H$ phase diagram for non-sticky chains is shown in Figure 5. A chain is assumed to be in a closed conformation if it fulfils the condition $|r_1 - r_N| < 3$. This definition is justified since $P_{Re}(x)$ depicts two well differentiated peaks in the bistable region: a narrow one centred around $x \approx 1$ and another one centred at values of $x > 10$, with a large difference between them (see Figure 4(b)). A more restrictive definition would result in an overestimate of the open chains due to thermal fluctuations. In order to determine the bistability region we have measured the probability of finding a chain in an open state, $P_o(\Gamma)$, in the point $\Gamma \equiv (H, T, \eta = 0, \mu^2 = 5, N = 100)$. Γ is assumed to be in the bistable region if $P_o \in [0.1, 0.9]$. It has been observed that reasonable variations of the threshold values do not change noticeably the results. The inset in Figure 5 zooms the region of small fields where the closed (ring-like) phase exists. At low fields the bistable region is very narrow, but as the external field increases the fluctuation region expands noticeably. The solid red line shows the boundary for the closed (ring-like) phase that exhibits a non-trivial behaviour.

3.2 Stockmayer filaments ($\eta > 0.0$)

In order to investigate the effect of the external magnetic field on Stockmayer filaments, we have selected the plane corresponding to $T = 0.5$ (see Figure 1). Several equilibrium conformations are observed depending on the values of (H, η) : open chains, closed ring-like structures, helix and compact globules. Representative examples of this conformations are illustrated in Figure 6. This figure also shows in addition how for a same set of parameters ($\eta = 0.05, H = 0.05, T = 0.5$) several types of conformations can be found to coexist in the case of sticky chains. Such multistability can be analysed through the evaluation of the pdf of the radius of gyration $f_{R_g}(x)$. The results for $H = 0.05$ and selected values of the stickiness η are shown in Figure 7. Note the existence of well defined peaks that can be associated to each observed structure. A

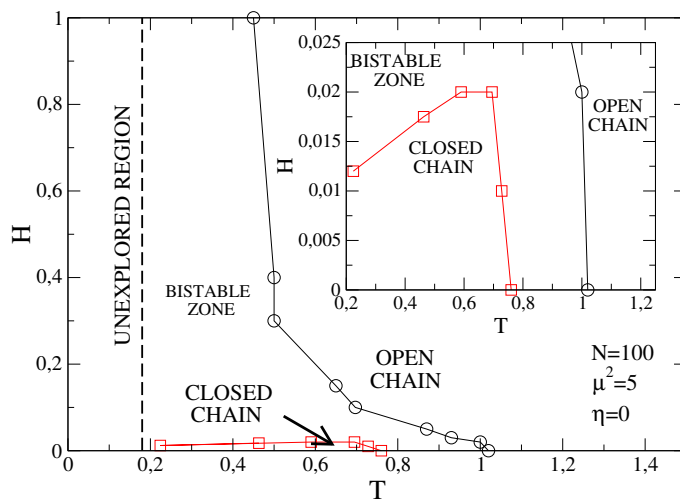


Fig. 5 $T - H$ phase diagram for non-sticky magnetic filaments. Closed structures are defined according to the criterion $|r_1 - r_N| < 3$. Bistable regions are defined by $P_o \in [0.1, 0.9]$ (see main text). The inset zooms the region of low temperatures and low field strengths.

first peak centred at $R_g \approx 20$ corresponds to open chains. A second peak located at $R_g \approx 10$ is related to a closed ring-like states. The last ones at $R_g \approx 5$ and $R_g \approx 3$ are associated to closed helices and compact globules, respectively.

The areas associated to each peak are directly related to the weight of each type of conformation in the multistate equilibrium and, therefore, it is possible to draw from them the probabilities of observing a Stockmayer filament in a certain position of the phase space $P_o(\Gamma)$, with $\Gamma \equiv (H, T = 0.5, \eta, \mu^2 = 5, N = 100)$. The results are presented in Figure 8. It can be clearly observed how an increase of H promotes the emergence of bistable and multistable regions. For small values of the stickiness parameter ($\eta \lesssim 0.05$), filaments that at zero-field adopt stable ring-like states, in the presence of a field fluctuate between ring-like and open (almost rod-like) conformations. At intermediate values ($0.05 \lesssim \eta \lesssim 0.09$), from the stable closed helicoidal state observed at zero-field, new structures emerge and coexist with it in the presence of an external field, such as, compact globules and, if the field is strong enough ($H \gtrsim 0.05$), open and closed ring-like conformations. For $\eta \gtrsim 0.09$, only compact globules are found within the range of H studied. The behaviour of the system for much larger values of H , in which open straightened chains are expected to be recovered, is presented below.

The overall message is that the equilibrium conformations of Stockmayer magnetic filaments and the coexistence of different phases are highly sensitive to small variations of the quality of the solvent (related to η) and the strength of the external field. As a consequence, structural properties, such as the average end-to-end distance, \bar{R}_{ee} , and radius of gyration, \bar{R}_g , can be modulated by tuning the values of η and H . The results are shown in Figure 9. From the picture it is possible to identify a threshold value of $\eta(H)$ that characterises the transition from large to small values \bar{R}_g corresponding to swollen or crumpled structures. The selection of one or another will strongly influence the rheological

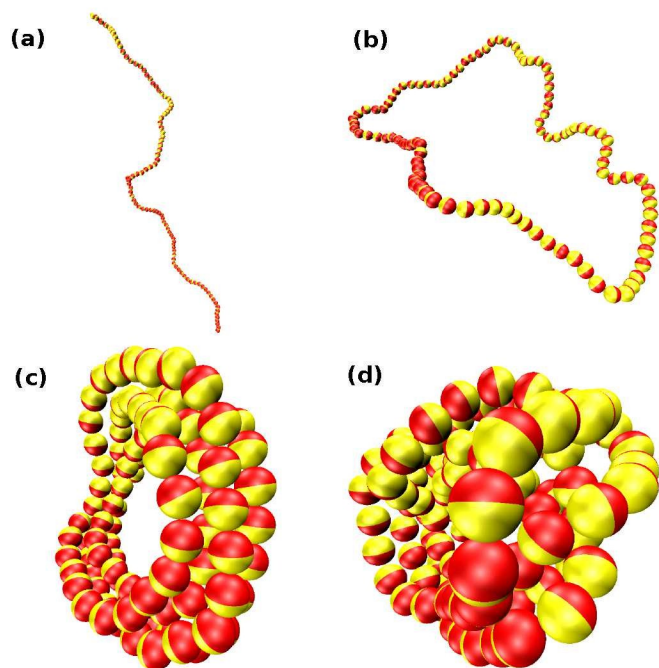


Fig. 6 Snapshots of a Stockmayer filament showing existence of multistability for $\eta = 0.05$ at $T = 0.5$ in the presence of an external magnetic field of strength $H = 0.05$. The vertical axis corresponds to the direction of the field, z -axis. Red and yellow semi-spherical caps help to display the orientation of the dipoles. From left to right and top to bottom: (a) open chain, (b) ring-like state, (c) closed helicoidal state, and (d) compact globule conformation. The rest of parameters are $\mu^2 = 5$ and $N = 100$.

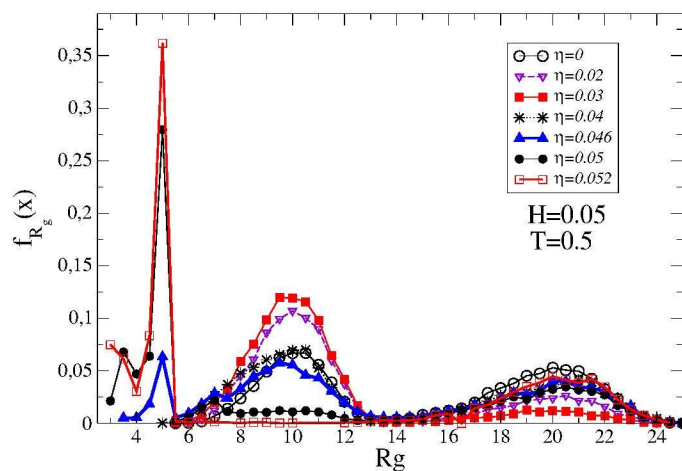


Fig. 7 Probability density function of the radius of gyration $f_{R_g}(x)$ for a Stockmayer polymer of length $N = 100$ and $\mu^2 = 5$ at different values of the stickiness η . The system temperature is set to $T = 0.5$ and the strength of the external field to $H = 0.05$.

properties of a magnetically responsive fluid containing such kind of filaments.

As pointed above, in the regime $\eta \gtrsim 0.09$ only compact globules are found for $H < 0.05$, and much larger values of the field are required to induce the transformation into other states. In the following, we will investigate the behaviour of the magnetic filament under strong fields along the direction in the phase space $\Gamma \equiv (H, T = 0.5, \eta = 0.2, \mu^2 = 5, N = 100)$. (see pink arrow in Figure 1). A summary of the results are presented in Figures 10 and 11. In Figure 10 we have measured the behaviour of several observables: the normalised averaged end-to-end distance \bar{R}_{ee}/N and radius of gyration \bar{R}_g/N ; the probability of finding open structures P_o , calculated according to the criteria followed in previous section, $|\mathbf{r}_1 - \mathbf{r}_N| < 3$, and the specific heat C_V that, for the sake of clarity, has been rescaled by a factor of 1000. In Figure 11 characteristic snapshots corresponding different conformational phases found for increasing values of H are presented.

It is possible to identify three regimes. For $H \lesssim 0.7$ the filament is typically in a compact globule state, characterised by small values of \bar{R}_{ee} and \bar{R}_g , and by a moderate increase in the probability of generating open structures ($P_o < 0.5$). In this regime the specific heat achieves its maximum value. An example is illustrated in Figure 11(a). A second regime can be easily described for $H \gtrsim 3$. The filament is found in an almost fully stretched configuration (see Figure 11(d)). $\bar{R}_{ee}/N \rightarrow 1$ and $\bar{R}_g/N \approx 1/\sqrt{12}$, the expected value for a rod. $P_o = 1$ and C_V has reached a plateau with its minimum value. In the transition regime ($0.7 \lesssim H \lesssim 3$), that is characterised by a monotonically decrease in the C_V and an increase in \bar{R}_{ee} and \bar{R}_g towards their final plateau values, we can differentiate two regions. For $0.7 \lesssim H \lesssim 1.5$, the filament is in a bistable region fluctuating between a compact globule configuration and a partially collapsed state (see Figures 11(b-c)). In this state the central part of the chain remains in a collapsed state, wrapping over itself, whereas the monomers near the ends are in straightened conformations. The probability of finding an open structure

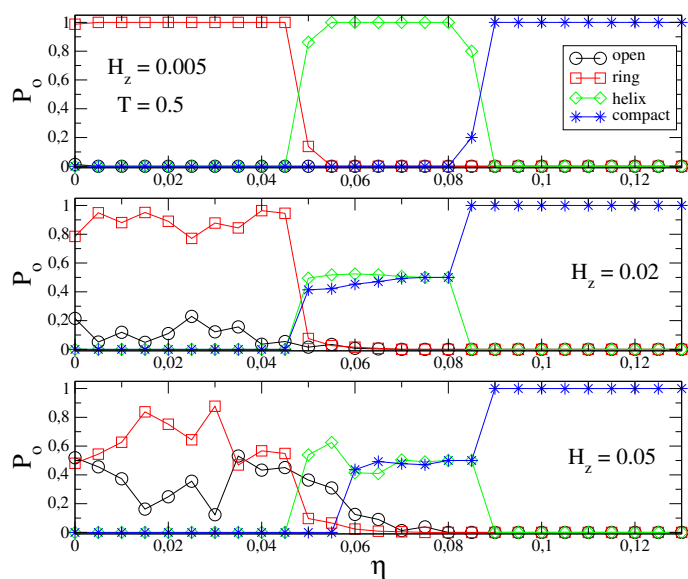


Fig. 8 Probability of finding a Stockmayer filament in different types of conformations as a function of the stickiness η for different values of the external field H . The rest of parameters are set to $N = 100$, $\mu^2 = 5$ and $T = 0.5$.

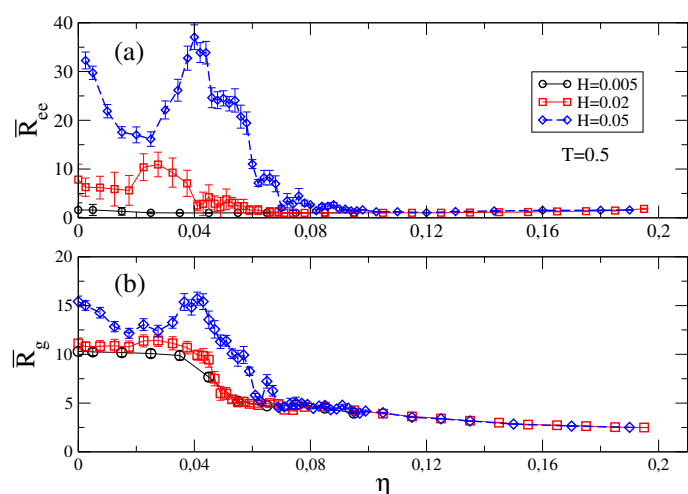


Fig. 9 Averaged end-to-end distance \bar{R}_{ee} (a) and radius of gyration \bar{R}_g (b) as a function of the stickiness η for different values of the external field H . The rest of the parameters are: $N = 100$, $\mu^2 = 5$ and $T = 0.5$. Error bars are plotted with a confidence interval of 95%.

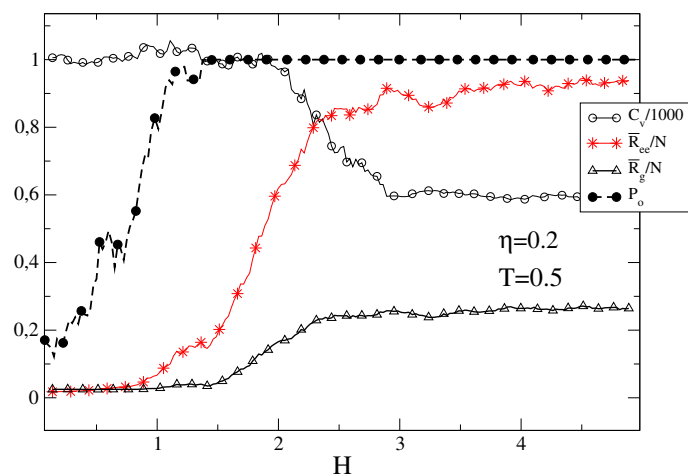


Fig. 10 Magnetic Stockmayer filament under the influence of strong magnetic fields. As a function of H several observables have been monitored: the normalised averaged end-to-end distance, \bar{R}_{ee}/N , and radius of gyration, \bar{R}_g/N ; the probability of finding open structures, P_o , and the rescaled specific heat, C_V . The rest of parameters are those of Figure 11.

increases until it reaches its maximum value $P_o = 1$. C_V and \bar{R}_g are barely affected, and a moderate increase in \bar{R}_{ee} is observed. Partially collapsed conformations are similar to those found at $H = 0$ at intermediate temperatures (see Figure 1). Finally, for $1.5 \lesssim H \lesssim 3$ there is a sharp expansion of the chain until it becomes fully unwrapped (see Figures 11(c-d)).

4 Conclusions

In this work it has been inferred, via extensive Langevin numerical simulations, how an external magnetic field modifies the conformational phase diagram of magnetic filaments in the limit of infinite dilution.

First, for a filament placed in a good solvent (stickiness set to $\eta = 0$) the phase diagram in the (H, T) plane has been investigated. At $H = 0$ we recovered previous results in which closed ring-like structures, at a reduced temperature $T \lesssim 0.8$, and open chains for $T \gtrsim 1$ are found⁴⁴. A small coexistence region is limited to $0.8 \lesssim T \lesssim 1$. For $H > 0$ we have been able to identify a threshold field value ($H_C \approx 0.02$) beyond which the results are clearly different from the zero-field case. Closed structures are limited to a non trivial region $H < H_C$ and $T \lesssim 0.8$. For $H > H_C$ a large bistable region emerges in which the magnetic filament fluctuates between open and closed conformations, see Figure 5. As expected, the transition line between the bistable region and the open chains one is displaced towards smaller temperatures as H increases. These results are fully supported by the analysis of the radius of gyration probability density, $f_{R_g}(x)$, and the end-to-end distance cumulative distribution functions $F_{R_{ee}}(x)$. Similar results have been observed by Danilov et al.⁵⁸ in the case of ferrofluids in the limit $T \rightarrow 0$ where a two-fold state is found.

On the other hand, filaments in poor solvents ($\eta > 0$) exhibit a far more intricate scenario. Several equilibrium conformations, including open chains, closed structures, helices and compact globules, are observed depending on the values of (H, η) in ei-

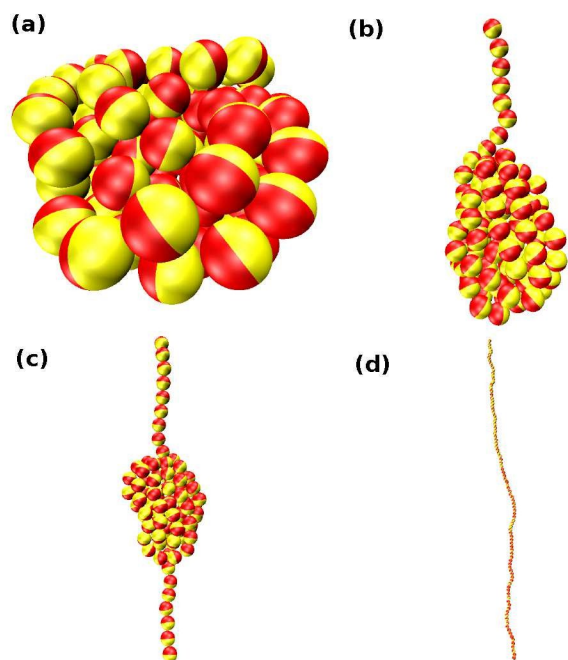


Fig. 11 Typical snapshots of the different conformational phases generated by an Stockmayer filament under strong fields. From left to right and top to bottom: (a) $H = 0.05$; (b) $H = 1.1$; (c) $H = 1.5$; (d) $H = 2.0$. The vertical axis corresponds to the magnetic field direction, z -axis. The rest of parameters are: $T = 0.5$, $\eta = 0.2$, $\mu^2 = 5$ and $N = 100$.

ther single domains or in multiple coexistence regions. For moderate field values ($H \leq 0.05$), in the region ($\eta \lesssim 0.05$), we observe a transition from a single closed domain to a bistable region in which rings coexist with open chains. For increasing values of the stickiness ($0.05 \lesssim \eta \lesssim 0.09$), single helicoidal states switch to a multiple domain in which all types of observed structures are present. Finally, for $\eta \gtrsim 0.09$, only compact globules are found. These results contrast with the zero-field case in which sharp transitions between rings to helices and from helices to compact globules take place and no multistability is observed at temperatures as low as $T = 0.5^{44}$.

Compact globules in fairly poor solvents ($\eta = 0.2$) can be destabilised with increasing values of the external field H . After a coexistence region with partially collapsed states, the system evolves towards a single domain characterised by fully stretched (rod-like) filaments. This transition pathway does not produce any helicoidal phase and it is far from what is naively expected from the zero-field results.

An explanation to such a variety of coexistence phases can be easily provided. For $H > 0$ the Zeeman contribution to the free energy substantially reduces the energy difference between competing conformations to the point where an effective reversible equilibria between those different states exist, even far away from any phase transition line.

Remarkably, the presence of even very moderate fields greatly enhances the possibility of tuning the properties of the filament by performing slight variations of the temperature or the solvent conditions, providing an unique opportunity to modulate and tai-

lor the average behaviour of the filaments.

The knowledge and control of the different types of structures that magnetic filaments may adopt is a key step in the determination of the properties of finite concentrations, as well as for other potential applications as nanoactuators, brushes or magnetic memories. We expect the present work will stimulate further developments on this field of increasing scientific interest.

Acknowledgements

This work was supported by the Conselleria d'Innovació, Recerca i Turisme del Govern de les Illes Balears and the European Social Fund (contract to JC). We also thank the Junta de Andalucía for its support via P11-FQM-7074 project (Spain). Simulations were performed at the IFISC's Nuredduna high-throughput computing clusters, supported by the project GRID-CSIC (ref.200450E494). TS and JJC also acknowledges FIS2012-30634 (funded by the Spanish MINCINN and the ERDF). SSK and PS thank the Austrian Research Fund (FWF): START-Projekt Y 627-N27. Partial support of ETN-COLLDENSE (H2020-MCSA-ITN-2014, Grant No. 642774) is acknowledged. S.S.K. is supported by RFBR mol-a-ved 15-32-20549.

References

- 1 C. Goubault, P. Jop, M. Fermigier, J. Baudry, E. Bertrand and J. Bibette, *Phys. Rev. Lett.*, 2003, **91**, 260802.
- 2 C. Goubault, F. Leal-Calderon, J.-L. Viovy and J. Bibette, *Langmuir*, 2005, **21**, 3725–3729.
- 3 F. Martínez-Pedrero, M. Tirado-Miranda, A. Schmitt and J. Callejas-Fernández, *Phys Rev E*, 2007, **76**, 011405.
- 4 B. A. Evans, A. R. Shields, R. L. Carroll, S. Washburn, M. R. Falvo and R. Superfine, *Nano Lett*, 2007, **7**, 1428–1434.
- 5 F. Martínez-Pedrero, M. Tirado-Miranda, A. Schmitt and J. Callejas-Fernández, *J. Colloid. Int. Sci.*, 2008, **318**, 23–28.
- 6 Y. Liu and Q. Chen, *Nanotechnology*, 2008, **19**, 475603.
- 7 H. Singh, P. E. Laibinis and T. A. Hatton, *Nano Letters*, 2005, **5**, 2149–2154.
- 8 J. J. Benkoski, S. E. Bowles, R. L. Jones, J. F. Douglas, J. Pyun and A. Karim, *Journal of Polymer Science Part B: Polymer Physics*, 2008, **46**, 2267–2277.
- 9 Z. Zhou, G. Liu and D. Han, *ACS Nano*, 2009, **3**, 165–172.
- 10 J. J. Benkoski, J. L. Breidenich, O. M. Uy, A. T. Hayes, R. M. Deacon, H. B. Land, J. M. Spicer, P. Y. Keng and J. Pyun, *J Mater Chem*, 2011, **21**, 7314–7325.
- 11 H. Wang, Y. Yu, Y. Sun and Q. Chen, *Nano*, 2011, **06**, 1–17.
- 12 D. Sarkar and M. Mandal, *J. Phys. Chem. C*, 2012, **116**, 3227–3234.
- 13 J. L. Breidenich, M. C. Wei, G. V. Clatterbaugh, J. J. Benkoski, P. Y. Keng and J. Pyun, *Soft Matter*, 2012, **8**, 5334–5341.
- 14 E. Busseron, Y. Ruff, E. Moulin and N. Giuseppone, *Nanoscale*, 2013, **5**, 7098–7140.
- 15 J. Byrom, P. Han, M. Savory and S. L. Biswal, *Langmuir*, 2014, **30**, 9045–9052.
- 16 L. J. Hill and J. Pyun, *ACS Applied Materials & Interfaces*, 2014, **6**, 6022–6032.

- 17 M. Kamachi, *J Macromol Sci-Pol R*, 2002, **C42**, 541–561.
- 18 S. J. Blundell and F. L. Pratt, *J Phys-Condens Mat*, 2004, **16**, R771–R828.
- 19 J. Liu, Y. Mao and J. Ge, *Nanoscale*, 2012, **4**, 1598–1605.
- 20 V. P. Shcherbakov and M. Winklhofer, *Phys. Rev. E*, 2004, **70**, 061803–na.
- 21 K. Ērglis, D. Zhulenkovs, A. Sharipo and A. Cēbers, *J Phys-Condens Mat*, 2008, **20**, 204107.
- 22 K. Ērglis, L. Alberte and A. Cēbers, *Magneto hydrodynamics*, 2008, **44**, 223–236.
- 23 S. L. Biswal and A. P. Gast, *Phys Rev E*, 2003, **68**, 021402.
- 24 A. Cēbers, *Curr Opin Colloid Interface Sci*, 2005, **10**, 167–175.
- 25 A. Cēbers and I. Javaitis, *Phys Rev E*, 2004, **69**, 021404.
- 26 M. Belovs and A. Cēbers, *Phys Rev E*, 2009, **79**, 051503.
- 27 M. Belovs, T. Ārulis and A. Cēbers, *J Phys A: Math Theor*, 2009, **42**, 235206.
- 28 A. Snezhko, M. Belkin, I. S. Aranson and W.-K. Kwok, *Phys. Rev. Lett.*, 2009, **102**, 118103.
- 29 K. I. Morozov and A. M. Leshansky, *Nanoscale*, 2014, **6**, 12142a–12150.
- 30 J. J. Benkoski, R. M. Deacon, H. B. Land, L. M. Baird, J. L. Breidenich, R. Srinivasan, G. V. Clatterbaugh, P. Y. Keng and J. Pyun, *Soft Matter*, 2010, **6**, 602–609.
- 31 F. Fahrni, M. W. J. Prins and L. J. van IJzendoorn, *Lab Chip*, 2009, **9**, 3413–3421.
- 32 A. Babataheri, M. Roper, M. Fermigier and O. D. Roure, *Journal of Fluid Mechanics*, 2011, **678**, 5–13.
- 33 N. Akkilic, F. A. M. Leermakers and W. M. de Vos, *Nanoscale*, 2015, **7**, 17871–17878.
- 34 Y. N. Kaznessis, D. A. Hill and E. J. Maginn, *Macromolecules*, 1998, **31**, 3116–3129.
- 35 P. A. Sanchez, E. S. Pyanzina, E. V. Novak, J. J. Cerda, T. Sintes and S. S. Kantorovich, *Macromolecules*, 2015, **48**, 7658–7669.
- 36 I. Stankovic, M. Dasic and R. Messina, *Soft Matter*, 2016, –.
- 37 E. Pitard, T. Garel and H. Orland, *J.Phys. I France*, 1997, **7**, 1201–1210.
- 38 K. I. Morozov and M. I. Shliomis, *Ferrofluids, Magnetically Controllable Fluids and Their Application*, Springer-Verlag, Heidelberg, 2002, pp. 162–184.
- 39 P. A. Sánchez, J. J. Cerdà, V. Ballenegger, T. Sintes, O. Piro and C. Holm, *Soft Matter*, 2011, **7**, 1809–1818.
- 40 C. Phatak, R. Pokharel, M. Beleggia and M. D. Graef, *J Magn Magn Mater*, 2011, **323**, 2912–2922.
- 41 P. A. Sánchez, J. J. Cerdà, T. Sintes and C. Holm, *The Journal of Chemical Physics*, 2013, **139**, 044904.
- 42 P. A. Sánchez, J. J. Cerdà, T. M. Sintes, A. O. Ivanov and S. S. Kantorovich, *Soft Matter*, 2015, **11**, 2963–2972.
- 43 A. F. Pshenichnikov and A. A. Kuznetsov, *Phys. Rev. E*, 2015, **92**, 042303.
- 44 J. J. Cerdà, P. A. Sánchez, C. Holm and T. Sintes, *Soft Matter*, 2013, **9**, 7185–7195.
- 45 J. D. Weeks, D. Chandler and H. C. Andersen, *J Chem Phys*, 1971, **54**, 5237–5247.
- 46 L. Hu, R. Zhang and Q. Chen, *Nanoscale*, 2014, **6**, 14064–14105.
- 47 R. M. Fratila, S. Rivera-Fernandez and J. M. de la Fuente, *Nanoscale*, 2015, **7**, 8233–8260.
- 48 M. P. Allen and D. J. Tildesley, *Computer Simulation of Liquids*, Clarendon Press, Oxford, 1st edn, 1987.
- 49 J. J. Cerdà, S. Kantorovich and C. Holm, *J Phys-Condens Mat*, 2008, **20**, 204125.
- 50 S. Kantorovich, J. J. Cerdà and C. Holm, *Phys Chem Chem Phys*, 2008, **10**, 1883–1895.
- 51 H. J. Limbach, A. Arnold, B. A. Mann and C. Holm, *Comput Phys Commun*, 2006, **174**, 704–727.
- 52 D. F. Parsons and D. R. M. Williams, *Phys Rev E*, 2006, **74**, 041804.
- 53 D. Seaton, T. Wüst and D. Landau, *Computer Physics Communications*, 2009, **180**, 587–589.
- 54 T. Vogel, M. Bachmann and W. Janke, *Phys Rev E*, 2007, **76**, 061803.
- 55 S. Schnabel, T. Vogel, M. Bachmann and W. Janke, *Chem Phys Lett*, 2009, **476**, 201 – 204.
- 56 T. A. Prokopyeva, V. A. Danilov, S. S. Kantorovich and C. Holm, *Phys Rev E*, 2009, **80**, 031404.
- 57 R. Messina, L. A. Khalil and I. Stanković, *Phys. Rev. E*, 2014, **89**, 011202.
- 58 V. Danilov, T. Prokopyeva and S. Kantorovich, *Phys. Rev. E*, 2012, **86**, 061408.